Numerical Simulation of Lake Breezes: Dependence on Location of Cloud Shadows on Land Surfaces

HOWARD W. BARKER*

Environment and Climate Change Canada, Victoria, BC, Canada

ZHIPENG QU

Environment and Climate Change Canada, Toronto, ON, Canada

YAOLUN YIN

University of Waterloo, Waterloo, ON, Canada

Submitted: xx December 2023

Revised: xx xxxx xxxx

For publication in: *J. Adv. Model. Earth Syst.*

* *Corresponding author address*: Howard Barker, Environment and Climate Change Canada, 2474 Arbutus Rd., Victoria, BC, Canada V8N 1V8 (howard.barker@ec.gc.ca).

Abstract

Simple parametrizations are developed that attempt to align high spatial-resolution distributions of surface solar irradiances predicted by 1D Independent Column Approximation (ICA) radiative transfer (RT) models with those from 3D RT models. Diffuse irradiances are smoothed to approximate horizontal diffusion below clouds, while direct-beam-induced cloud shadows are repositioned properly across the surface. Pearson correlation coefficients for global irradiances from a full 3D RT model and a 1D-ICA are ~0.2 and ~0.85 at low and high Sun, respectively. These values typically increase to ~0.87 and ~0.97 for the parametrization developed here.

Lake breezes that arise from solar heating of land surfaces are simulated by a Numerical Weather Prediction (NWP) model using 250 m horizontal grid-spacing and either its regular 1D-ICA solar RT model (*control*) or the 1D parametrization (*experiment*). Idealized conditions are: i) flat surfaces; ii) lake with uniform temperature and optical properties; iii) uniform land-type with variable temperature, moisture, and albedo; iv) infinitely long linear coastlines running E-W; v) cyclic boundary conditions in the N-S direction with alternating strips of land and lake at 30 km and 70 km wide, respectively; vi) uniform and constant imposed synoptic winds; and vii) solar geometry for 43° N latitude on 8-July. Simulations started at 8h00 local time and lasted 8 hrs. Five member ensembles were produced for *control* and *experiment*. While the NWP model's response to forcings set-up by the 1D parametrization are clear and explicable, differences to surface meteorological variables are minor and would not impact weather forecasts. Owing to the high solar-sensitivity of these conditions, these results suggest that short-range NWP forecasts would gain little from having their efficient 1D RT models replaced by expensive 3D counterparts. This claim cannot, as yet, be extended to either seasonal forecasts or climate simulations.

1. Introduction

Sea breezes span a variety of sizes and strengths. At the top end are regional monsoons that usually last several months (e.g., the Indian Monsoon). At the bottom, localized lake breezes usually last less than half a day. All such breezes are characterized by low-level flows of air from a cool body of water that are drawn onto relatively warm adjacent land where temperatures are elevated by solar radiative heating. Lake breezes frequent the coasts of North America's Great Lakes during late-spring and summer. Shortly after mid-day, when surface solar irradiances maximize, convective clouds form along the leading edge(s) of a lake breeze as moist low-level air from over the lake ascends, cools, and condenses. In some cases, cells of intense convective precipitation occur. Locally reduced surface temperatures due to cloud shadows, and possibly precipitation, throttle-down lake breeze circulation thereby suppressing convection and cloud formation. With fewer clouds, surface solar irradiance can increase near the weakened breeze-front, which can reinvigorate it thus affecting a localized feedback process (cf. Gronemeier et al. 2017).

Numerical simulations of sea and lake breezes have been performed for many decades (e.g., Estoque 1961; Das 1980). When run with sufficiently small horizontal grid-spacings Δx, numerical weather prediction (NWP) models simulate lake breezes well (Dehghan et al. 2018). NWP models compute solar fluxes, however, with 1D solutions of the radiative transfer (RT) equation, and so clouds cast shadows into nadir regardless of solar zenith angle θ_0. Application of 1D RT models to each column of a discretized domain is known as the Independent Column Approximation (ICA) (e.g., Barker and Davis 2005). As the 1D-ICA often yields accurate temporal-spatial integrals of surface radiation budgets (e.g., Hogan et al. 2019), it is not surprising that the basic features of monsoons can be simulate well. For localized, short-lived lake breezes, however, use of the 1D-ICA might be problematic due to confinement of cloud shadow to nadir. Indeed, some studies suggest that 3D RT effects can be important when simulating shallow cumulus clouds (Schumann et al. 2002; Wapler and Mayer 2008; Jakub and Mayer 2017). ***Figure 1*** illustrates this issue for Sun shining from the NW at $\theta_0 = 45°$ and nadir-viewing (from satellite). In (a), 3D RT was performed, so shadows cast by clouds towards the SE are readily apparent. In (b), however, 1D-ICA RT was performed, so all cloud shadows are hidden from view (perpetual opposition effect).

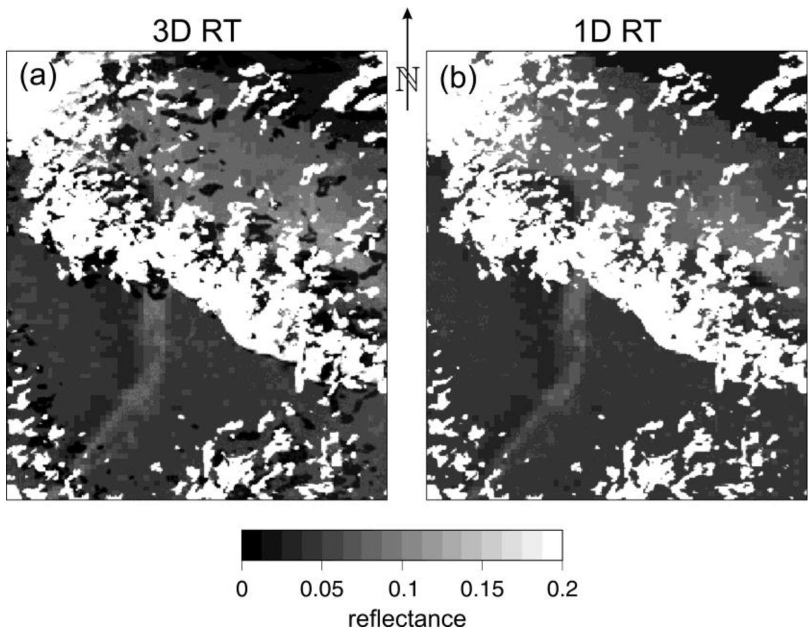

Figure 1. (a) Nadir-view of clouds (saturated white) above the NE coast of South America computed by a 3D solar RT model with the Sun coming in from the NW at $\theta_0 = 45°$. (b) As in (a) except this was computed by a 1D RT model in ICA-mode.

The purpose of this study is to explore whether the 1D-ICA's improper projection of cloud shadows impacts simulation of lake breezes for conditions resembling those near the Great Lakes of Southern Ontario. Experiments were performed with the Global Environmental Multi-scale (GEM) NWP model using first its regular ICA solar RT model, and then simple adjustments to ICA direct- and diffuse-beam surface irradiances. A full 3D solar RT model was not used for two reasons: i) domain-average flux profiles computed by 1D-ICA models are often very good approximations of their 3D RT model counterparts (e.g., Hogan et al. 2019); and ii) for domains as large as those used here, computer resources needed to perform simulations with a un-optimized 3D RT model would far exceed those used by the 1D-ICA; which already accounts for a significant portion of the NWP model's run-time (per. comm., P. Vaillancourt 2018). Nevertheless, these experiments should help establish the need to perform more extensive tests involving full 3D RT models.

The following section describes adjustments to ICA surface solar irradiances that aim to mimic 3D RT values. These are assessed, in the third section, against 3D RT model results for a range of partly cloudy model atmospheres. The fourth section provides a brief description of NWP model used here for lake breeze experiments. This is followed by results and a conclusion.

2. A simple transformation of ICA surface solar irradiances

The underlying assumption going into this study was that poor estimation of 2D distributions of solar heating over land by 1D-ICA RT models adversely impacts forecasts of lake breezes. To facilitate tractable experiments aimed at helping establish whether NWP models should replace their ubiquitous 1D solar RT models for more costly 3D solutions, simple adjustments to 1D-ICA surface solar irradiances are proposed and explained in this section. Consider first, however, the motivation behind the proposed adjustments.

2.1. Parametrization motivation

Results shown in this section, and in §3, were produced by applying a 3D Monte Carlo solar RT model, with gaseous attenuation properties based on the RRTMG model (Iacono et al. 2008), to sixty-five (100 km)^2 model-generated cloudy-sky domains above uniform ocean with horizontal grid-spacing $\Delta x = 250$ m. These domains, and the RT model, were also used by Hogan et al. (2019) and were extracted from two large simulations: one from Greenland to Dominican Republic on 7 December 2014, and the other from Hawaii to Tonga on 24 June 2015. (Illingworth et al. 2015; Qu et al. 2023). Full 3D RT benchmarks used $\Delta x = 250$ m, while their 1D-ICA counterparts used $\Delta x = 10^6$ m, which affects the ICA via near-complete elimination of photon exchange amongst columns.

While several studies have highlighted pathological differences in domain-average solar fluxes estimated by 1D and 3D solar RT models for select cloud scenarios (e.g., Barker et al. 1999), more holistic studies, that considered wide ranges of cloud forms, arrived at differences for surface fluxes that are typically less than ± 20 W m^{-2} (e.g., Ham et al. 2014; Barker et al. 2016; Hogan et al. 2019; Gristey et al. 2020; Cole et al. 2023). These are echoed in ***Figure 2*** which shows a repackaging of Hogan et al.'s (2019) results. ***Figure 2a*** and ***Figure 2c*** show median and standard percentile values for domain-average global irradiance and solar heating rates, at cosine of solar zenith angle $\mu_0 = \cos\theta_0 = 0.5$, where is θ_0 solar zenith angle, computed by the 3D RT model for all 65 domains. Comparing these two plots to their counterparts on the right shows that differences between 1D and 3D RT, at these scales, are much smaller than their median values. For both surface irradiance and heating rates, 1D - 3D differences are usually less than 1%.

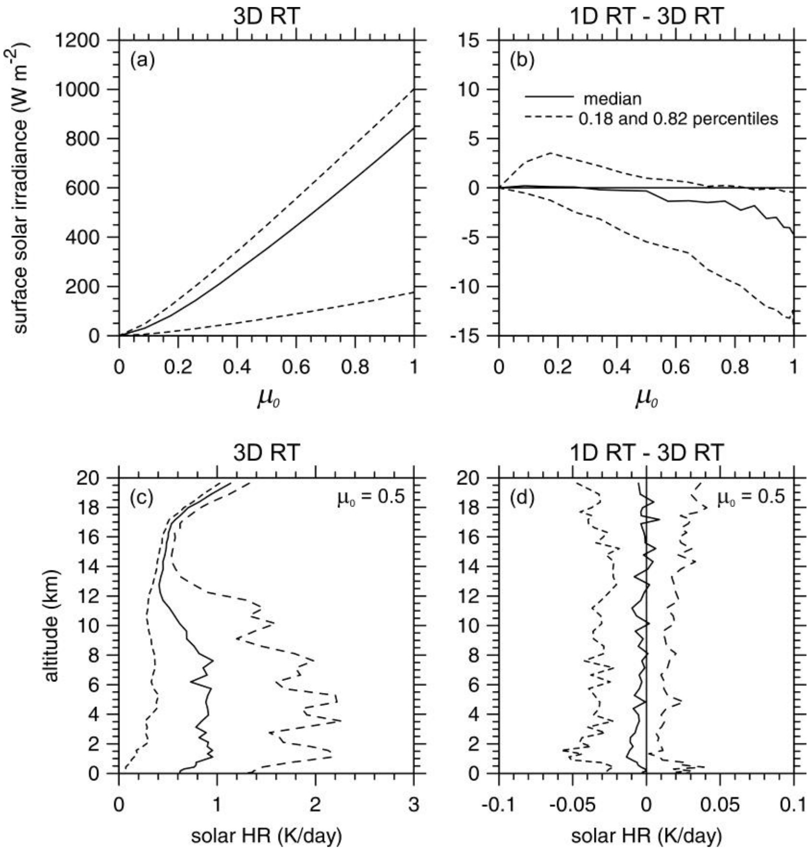

Figure 2. (a) Solid line is median of domain-average surface solar irradiance for 65 domains (see text) as a function of cosine of solar zenith angle μ_0. Dashed lines are corresponding 0.18 and 0.82 percentiles (~66% of cases are between these lines; cf. standard deviation). (b) As in (a) except these are for differences between 1D and 3D RT results. (c) As in (a) except these are for HRs at $\mu_0 = 0.5$. (d) As in (b) except these are for heating rate differences.

Compare now values in ***Figure 2*** to those in ***Figure 3*** which shows, for a single typical domain, 1D RT global irradiances against their 3D counterparts when averaged up to 1 km resolution (which reduces Monte Carlo uncertainty by a factor of ~4). For $\theta_0 = 0°$ (overhead Sun), 1D and 3D domain-averages differ by ~1%, as in ***Figure 2***, but locally they differ typically by ~10%. This is due to horizontal diffusion of radiation scattered by clouds in the downwelling direction. At $\theta_0 = 60°$, domain-averages still differ by only ~1% but locally they differ usually by ~30%. This is due primarily to massively incorrect placement of direct-beam irradiance by 1D RT.

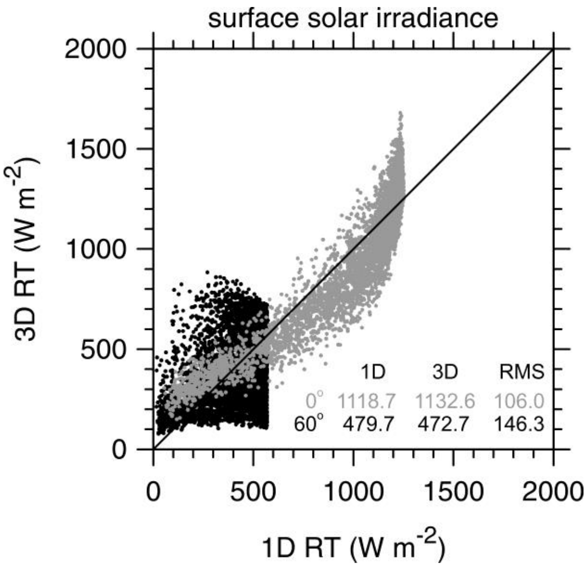

Figure 3. Each dot represents an ordered pair of surface solar irradiances for a 1 km square for a single domain as predicted by 1D RT and 3D RT. Grey and black dots are for $\theta_0 = 0°$ and $60°$, respectively. Listed values are domain averages for both RT models with "RMS" standing for root mean-square difference between the two at 1 km resolution.

The null hypothesis arising from these results, and motivated development of the following parametrization, is: neglect by NWP models of 3D solar RT effects in the sub-mesoscale range outweigh corresponding errors at larger scales and does not affect weather forecasts.

2.2. Parametrization development

Define domain-average global surface irradiance predicted by a 1D solar RT model as

$$\begin{aligned}\langle G(\mu_0)\rangle &= \langle d(\mu_0)\rangle + \langle D(\mu_0)\rangle \\ &= (1-A_c)\left[\langle d_{clr}(\mu_0)\rangle + \langle D_{clr}(\mu_0)\rangle\right] + A_c\left[\langle d_{cld}(\mu_0)\rangle + \langle D_{cld}(\mu_0)\rangle\right],\end{aligned} \quad (1)$$

where $\langle d\rangle$ and $\langle D\rangle$ are domain-average diffuse- and direct-beam irradiances, A_c is vertically-projected total cloud fraction, $\langle d_{clr}\rangle$ and $\langle d_{cld}\rangle$ are mean diffuse-beam irradiances for the cloudless and cloudy portions of the domain, respectively, and $\langle D_{clr} \rangle$ and $\langle D_{cld} \rangle$ are their direct-beam counterparts. Correspondingly, results from a full 3D RT model can be cast as

$$\begin{aligned} \langle G'(\mu_0,\varphi_0) \rangle &= \langle d'(\mu_0,\varphi_0) \rangle + \langle D'(\mu_0,\varphi_0) \rangle \\ &= \left[1 - A_c'(\mu_0,\varphi_0)\right]\left[\langle d_{clr}'(\mu_0,\varphi_0) \rangle + \langle D_{clr}'(\mu_0,\varphi_0) \rangle\right] \\ &\quad + A_c'(\mu_0,\varphi_0)\left[\langle d_{cld}'(\mu_0,\varphi_0) \rangle + \langle D_{cld}'(\mu_0,\varphi_0) \rangle\right], \end{aligned} \tag{2}$$

where φ_0 is solar azimuth angle, and $A_c'(\mu_0,\varphi_0)$ is cloud fraction presented to the direct-beam, in which $A_c'(\mu_0 = 1) = A_c$. This is also the interpretation of the 1D ICA parametrization.

The first assumption in the 1D ICA parametrization is that 3D RT diffuse-beam fields can be approximated by simply smoothing their 1D RT compeers and constraining

$$\langle d(\mu_0) \rangle = \langle d'(\mu_0,\varphi_0) \rangle. \tag{3}$$

This allows (2) to be rewritten as

$$\begin{aligned} \langle G'(\mu_0,\varphi_0) \rangle &= \langle d(\mu_0) \rangle + \left[1 - A_c'(\mu_0,\varphi_0)\right]\langle D_{clr}'(\mu_0,\varphi_0) \rangle \\ &\quad + A_c'(\mu_0,\varphi_0)\langle D_{cld}'(\mu_0,\varphi_0) \rangle. \end{aligned} \tag{4}$$

Admittedly, under some conditions, (3) can be extreme (e.g., Barker et al. 1999).

The second, and easily justifiable, assumption is that *mean* cloudless-sky direct-beam irradiances are equal for 1D and 3D RT. This, as in (3), implies that

$$\langle D_{clr}(\mu_0) \rangle = \langle D_{clr}'(\mu_0,\varphi_0) \rangle. \tag{5}$$

Next, assume further that domain-average global irradiances for the default and parametrized 1D RT models are equal. Thus, substituting

$$\langle G(\mu_0)\rangle = \langle G'(\mu_0,\varphi_0)\rangle \tag{6}$$

into (4) and using (5), mean cloudy-sky direct-beam irradiance for the parametrization is

$$\langle D'_{cld}(\mu_0,\varphi_0)\rangle = \frac{\langle G(\mu_0)\rangle - \langle d(\mu_0)\rangle - \left[1 - A'_c(\mu_0,\varphi_0)\right]\langle D_{clr}(\mu_0)\rangle}{A'_c(\mu_0,\varphi_0)}, \tag{7}$$

where everything on the RHS, save for $A'_c(\mu_0,\varphi_0)$, comes from the usual application of the 1D RT model. The following two subsections describe estimation of $A'_c(\mu_0,\varphi_0)$ and definition of spatial distributions of diffuse- and direct-beams for the parametrized 1D model.

2.3. Direct-beam irradiance and μ_0-dependent cloud fraction

A ray-tracing algorithm, pared-down from Barker et al.'s (2003) Monte Carlo algorithm, is used to approximate $A'_c(\mu_0,\varphi_0)$ and the location of parametrized direct-beam irradiance onto the surface. From the centre of each surface grid-cell at (i,j), a single ray is traced toward the Sun and visible optical depth of cloud $\tau'_{cld}(i,j;\mu_0,\varphi_0)$ accumulated along it. This leads to location-dependent direct-beam transmittances for clouds defined as

$$T'_{cld}(i,j;\mu_0,\varphi_0) = \begin{cases} \exp\left[-\tau'_{cld}(i,j;\mu_0,\varphi_0)\right] & ; \quad \tau'_{cld} > \tau_{crit} \\ 1 & ; \quad \tau'_{cld} \le \tau_{crit}. \end{cases} \tag{8}$$

Hereinafter, $\tau_{crit} = 0.1$ was used. To ensure (6), direct-beam irradiance at a cloudy cell (i,j) for the parametrized model is

$$D'_{cld}(i,j;\mu_0,\varphi_0) = \left[\frac{\langle D'_{cld}(\mu_0,\varphi_0)\rangle}{\langle T'_{cld}(i,j;\mu_0,\varphi_0)\rangle}\right] T'_{cld}(i,j;\mu_0,\varphi_0). \tag{9}$$

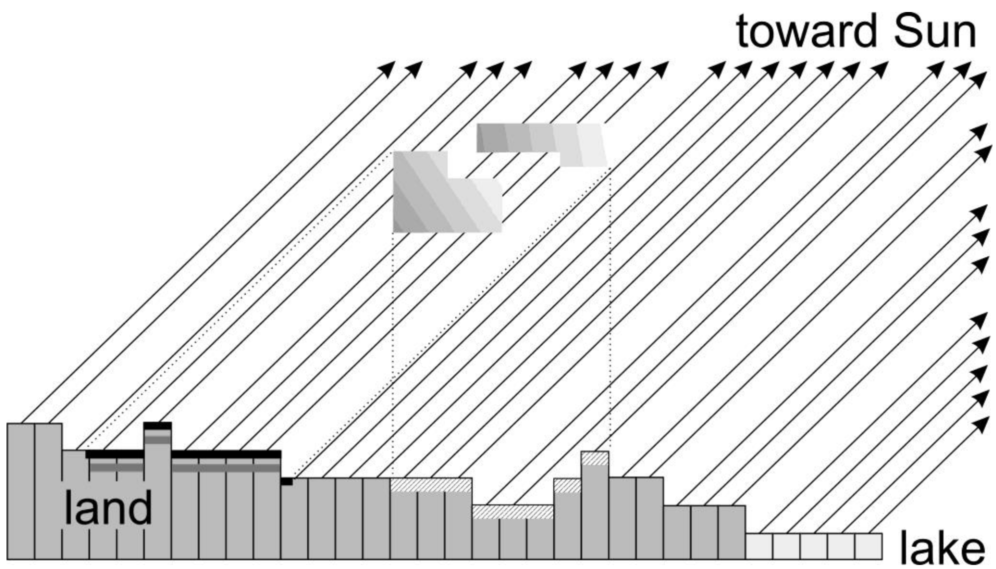

Figure 4. Schematic of the surface centre-point ray tracing algorithm used to estimate total cloud fraction presented to direct-beam A_c', T_{cld}' (see (8)), and location of cloud shadows. Location of true cloud shadows are indicated in black while those for the 1D-ICA parametrization are dark grey. Cloud shadows for the true 1D-ICA are stippled bands.

For a domain of $N \times N$ columns, directional-dependent total cloud fraction presented to direct-beam is

$$A_c'(\mu_0, \varphi_0) = \frac{1}{N^2} \sum_{i=1}^{N} \sum_{j=1}^{N} \Phi\left[\tau_{cld}'(i, j; \mu_0, \varphi_0)\right], \tag{10}$$

where

$$\Phi[x] = \begin{cases} 0 & ; \quad x \le \tau_{crit} \\ 1 & ; \quad x > \tau_{crit}. \end{cases} \tag{11}$$

Figure 4 shows a schematic of this procedure. From this simply illustration one can easily appreciate that for small horizontal grid-spacings, errors in shadow locations and A_c' will be small.

2.4. Diffuse-beam irradiance

Denote 2D distributions of diffuse irradiance computed by 3D and 1D solutions of the RTE as $d'(i,j;\mu_0,\varphi_0)$ and $d(i,j;\mu_0)$, respectively. Since $d'(i,j;\mu_0,\varphi_0)$ consist of photons arriving from anywhere in the hemisphere, while $d(i,j;\mu_0)$ receives them only from directly above, a first-order approximation to $d'(i,j;\mu_0,\varphi_0)$ is to smooth $d(i,j;\mu_0)$. A very simplistic approach (cf. Marshak et al. 1995; Barker and Marshak 2001; Tijhuis et al. 2022) was taken here in which diffuse irradiance at (i,j) for the 1D-ICA parametrization (i.e., for 3D RT) is approximated as

$$d'(i,j;\mu_0) = \frac{\sum_{m=-\ell}^{\ell}\gamma(m)\,d(i+m,j;\mu_0) + \sum_{m=-\ell}^{\ell}\gamma(m)\,d(i,j+m;\mu_0)}{2\sum_{m=-\ell}^{\ell}\gamma(m)}, \qquad (12)$$

where

$$\gamma(k) = \cos^2\left(\frac{k\cdot\Delta x}{h'_{cld}}\right), \qquad (13)$$

ℓ corresponds to the number of cells removed from (i,j) where $\gamma(k) \le \gamma_{crit}$, and h'_{cld} is an "effective" cloud altitude. Maximum weight is always given to the zenith with less weighty contributions coming from neighbouring columns along two perpendicular tracks that intersect (i,j). For this study, γ_{crit} was set arbitrarily to 0.25. At this level of approximation, (12) is as justified as the more taxing use of all values of d in a circle of radius ℓ around (i,j).

Letting $\langle w_{cld}(k)\rangle$ be the k^{th} layer's domain-average cloud water content, and $\Delta z(k)$ be layer geometric thickness, h'_{cld} is defined as

$$h'_{cld} \equiv z\left(\arg\max_{k}\left[\langle w_{cld}(k)\rangle \Delta z(k)\right]\right). \tag{14}$$

This approximation has almost no impact for near-cloudless skies and only minor impacts for most overcasts. While a better description of h'_{cld} would see it depend on (i, j), its computation would not be justified for this level of approximation, and it could violate (3) and (6), which would upset experimental control. The final, and obvious, step is definition of local parametrized global irradiances being the addition of (12) to either $D'_{cld}(i, j)$ or $D_{clr}(i, j)$.

3. Results I: Radiative transfer parametrization

This section shows results for the RT parametrization presented in §2. All results in this section were produced by applying a 3D Monte Carlo solar RT model, with gaseous attenuation properties based on the RRTMG model (Iacono et al. 2008), to sixty-five (100 km)^2 cloudy-sky domains, which were simulated by GEM, above a uniform ocean surface, with horizontal grid-spacing $\Delta x = 250$ m. These domains and the RT model (Cole et al. 2023) were also used in Hogan et al. (2019). Full 3D RT benchmarks used $\Delta x = 250$ m, while their 1D-ICA and parametrization counterparts used $\Delta x = 10^6$ m, which affects the ICA via near-elimination of photon exchange between columns. Each simulation used 10^8 photons per domain. These scenes are subsets of two large domains that were simulated by GEM for the purpose of assessing EarthCARE satellite retrieval algorithms (Illingworth et al. 2015; Qu et al. 2023): Greenland to Dominican Republic on 7-12-2014; Hawaii to Tonga on 24-6-2015.

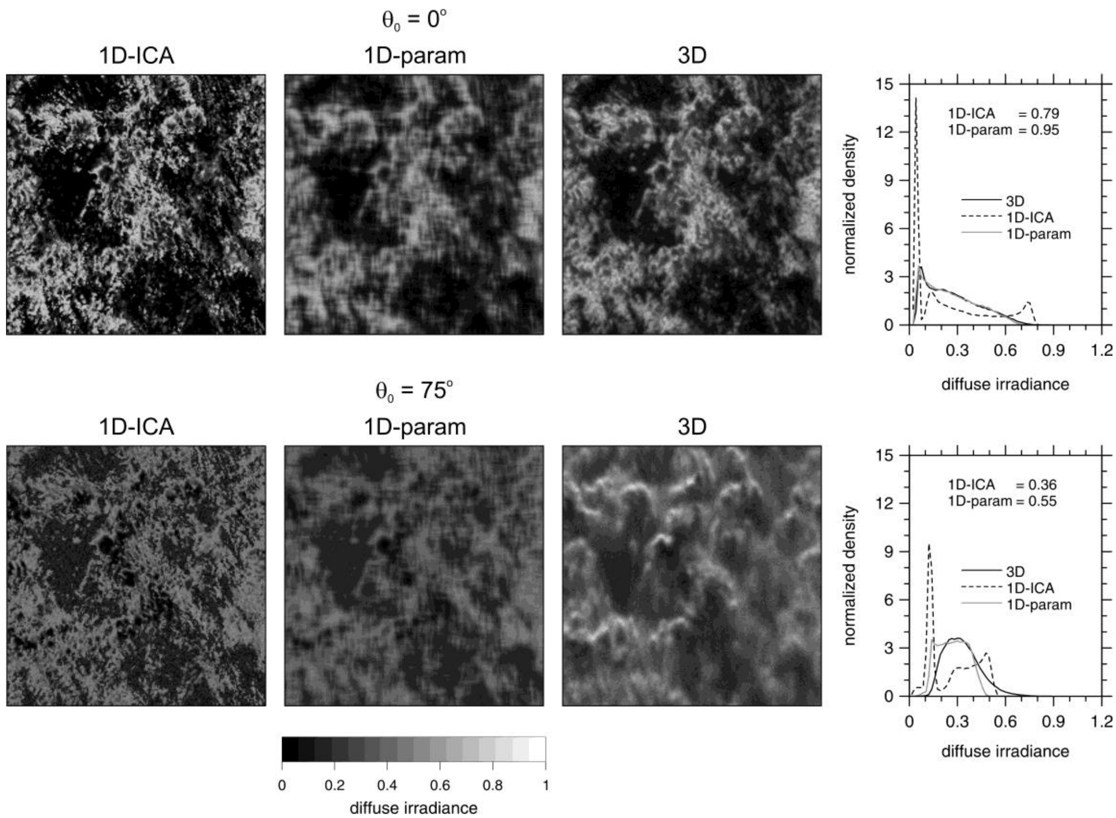

Figure 5. Upper row: Maps show surface diffuse irradiance, for overhead solar illumination ($\theta_0 = 0°$), across a (100 km)^2 domain, from the Atlantic swath, predicted by the 1D-ICA, modified 1D, and 3D RT models. Plot on the right shows distributions of values in the maps. Listed values are Pearson correlation coefficients between 1D RT and corresponding 3D values. Lower row: As in the upper except that $\theta_0 = 75°$ with Sun coming in from 12 o'clock.

Figure 5 shows maps of diffuse irradiance predicted by the 3D Monte Carlo, regular 1D-ICA, and parametrized ICA models for $\theta_0 = 0°$ and $\theta_0 = 75°$. At $\theta_0 = 0°$, features in the 1D-ICA field are very "sharp", while those in the 1D-param field are overly diffuse relative to the 3D. Maps for the 1D and 1D-param at $\theta_0 = 75°$ look much the same as at $0°$, whereas the 3D map is altered much due to cloud side-illumination and shadows. Nevertheless, Pearson correlation coefficients *r* between 1D model results and 3D values, as listed on the adjacent line plots, indicate that the smoothed 1D-ICA fields track the 3D results substantially better than the regular 1D-ICA.

Density functions in ***Figure 5*** indicate that 1D RT local irradiances are often too small or too large; endless clear- or overcast-skies, respectively. The smoothing process described in §2.4, however, yields distributions that agree extremely well with the 3D model's. Note that the relatively long tail for 3D RT at $\theta_0 = 75°$ stems from enhanced interception of direct-beam radiation by clouds and the ensuing concentrating of radiation scattered downward onto nearby ground.

Figure 6 is like ***Figure 5*** except it shows global surface irradiances. Clearly, maps of parametrized 1D results resemble the 3D maps much better than do the regular 1D-ICA. This is reflected in *r* which tend to increase by 0.4 to 0.6 thanks to the vast improvement in positioning of direct-beam irradiance across the domain. As with the diffuse fields, frequency distributions for 1D-param resemble closely those for the 3D RT, while the regular 1D-ICA's distributions are remarkably narrow (cf. Barker et al. 2017).

Figure 7 shows mean and standard deviations of *r* for fields of surface irradiances for the 1D-ICA and 1D-param models relative to their 3D RT counterparts as functions of μ_0 for all 65 (100 km)^2 domains. For diffuse irradiance, parametrized 1D values of *r* are about 0.2 larger than those for the 1D-ICA, regardless of θ_0 (cf. ***Figure 5***). More importantly, especially for non-overcast domains, direct-beam for 1D-param are almost perfectly correlated with the 3D benchmarks, and this translates into values of *r* between 1D-param and 3D fields rarely being less than 0.8 and always being much larger than those for the regular 1D-ICA model.

In summary, biases incurred by 1D-ICA RT models most in need of addressing are those at small-scales for partly cloudy skies. To this end, the simple adjustment to 1D-ICA surface irradiances should suffice in exploring the impact of neglecting, expensive to obtain, 3D RT effects. The following sections do this for solar-driven lake breeze conditions.

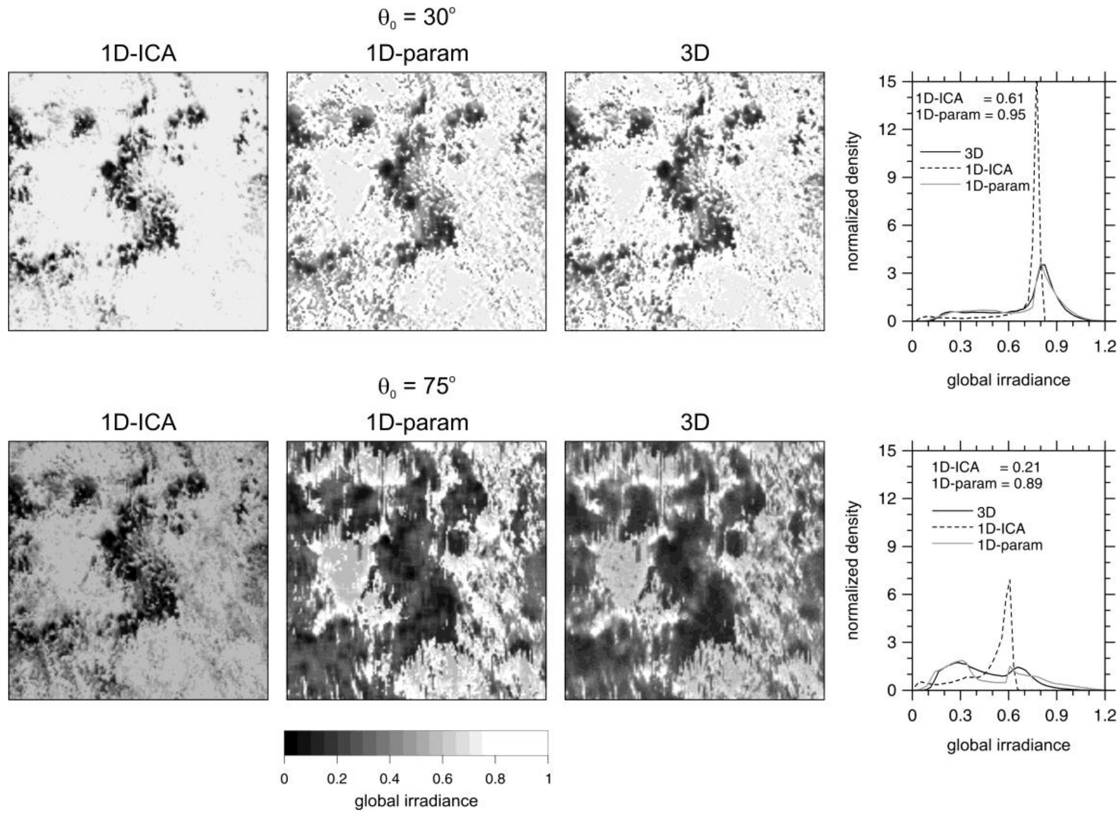

Figure 6. As in ***Figure 5*** but these are for surface global irradiances at $\theta_0 = 30°$ and $\theta_0 = 75°$.

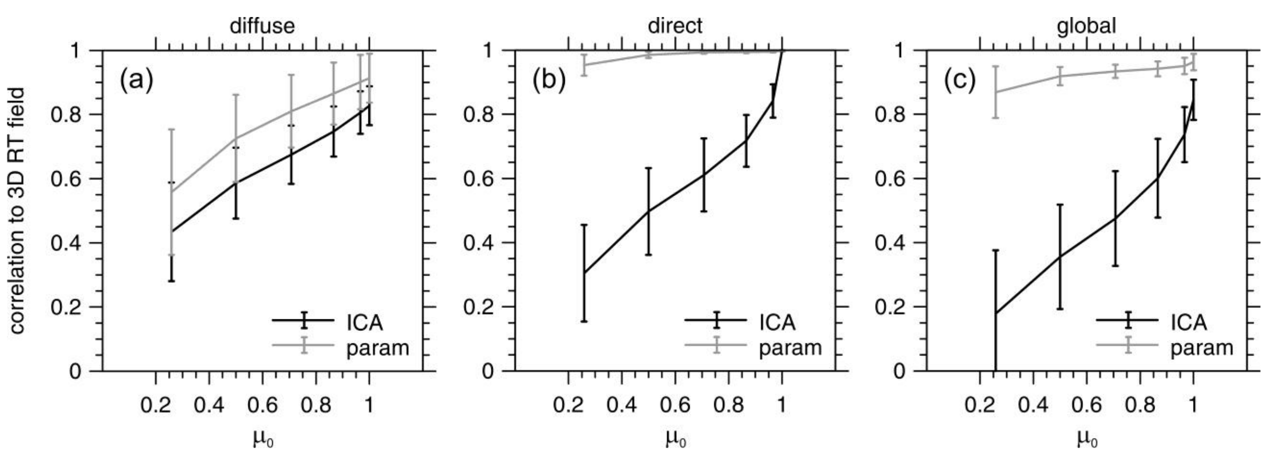

Figure 7. Pearson correlation coefficients *r* between 2D fields of diffuse, direct, and global surface irradiances predicted by the ICA and the parametrized ICA RT models relative to their 3D RT counterparts, as functions of μ_0. Solid lines indicate mean values for the 65 scenes considered in this portion of this study. Corresponding standard deviations are indicated by the bars.

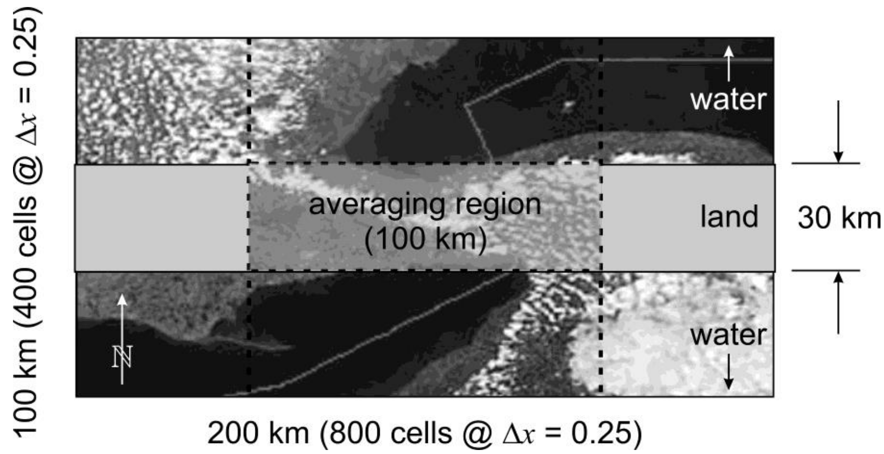

Figure 8. Schematic showing GEM's inner-domain (200 km x 100 km) with a 30 km-wide strip of land bordered by water. It is superimposed on a satellite image of the Niagara region between Lakes Ontario and Erie. For analyses, only the central 100 km x 30 km portion is considered.

4. NWP model simulation of lake breezes

For this study, ECCC's Global Environmental Multiscale (GEM) NWP model was used (Côté et al. 1998; Girard et al. 2014). For details, including radiation and cloud-precipitation microphysics, see McTaggart-Cowan et al. (2019). GEM is usually run with four one-way nested domains (Milbrandt et al. 2016; Bélair et al. 2017). Experiments reported here, however, were performed with an idealized version using $\Delta x = 0.25$ km and 57 vertical layers with inner-domain measuring 200 km east-west by 100 km north-south. There was a continuous and homogenous strip of land running east-west that was 30 km north-south. Uniform water bordered it, and the entire domain was set in a larger water surface domain with $\Delta x = 1$ km. As ***Figure 8*** shows, this configuration resembles the isthmus between Lakes Ontario and Erie where lake breezes are common. Domains were cyclic and analyses were restricted to the central 100 km of land. At the end of a time step, the 1D-ICA RT model's direct- and diffuse surface irradiance fields were either: i) used as usual (i.e., *control*); or ii) adjusted according to that described in §2 (*experiment*).

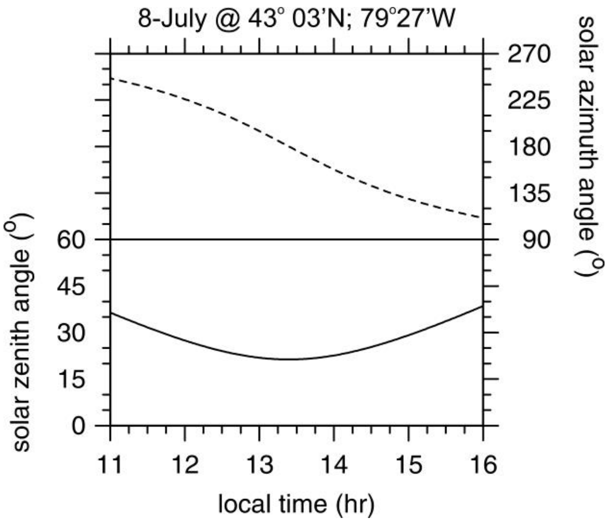

Figure 9. Solar zenith and azimuth angles as functions of local time for the date and location listed in the title. Solar noon occurs at about 13h20 (daylight saving time) when $\varphi_0 = 180°$.

All simulations started at 12h00 UTC using initial conditions from archived analysis for 8-July-2020. The centre of the domain corresponds to $(43° \, 03' \text{N}; 79° 27' \text{W})$, and ***Figure 9*** shows solar zenith and azimuth angles. Synoptic winds were imposed from the SW, NW, or W directions and fixed during simulations. For the W-wind, the westerly component was from analysis data and reduced by 50% in order to establish a lake breeze. The southerly component was set to 0. For SW and NW cases, the north/south component was prescribed at 25% of the westerly component. A fourth scenario had no synoptic wind. Most of the results shown in the following section pertain to the “no synoptic wind” and “SW” experiments because they capture the essential features and these conditions are common when lake breezes prevail near the Great Lakes.

For each wind direction five member ensembles were performed for both *control* and *experiment*. Each ensemble member had initial values of land surface temperatures, from analysis, perturbed by random Gaussian noise with standard deviation $1°\text{C}$. Water surface temperatures were fixed at $24°\text{C}$.

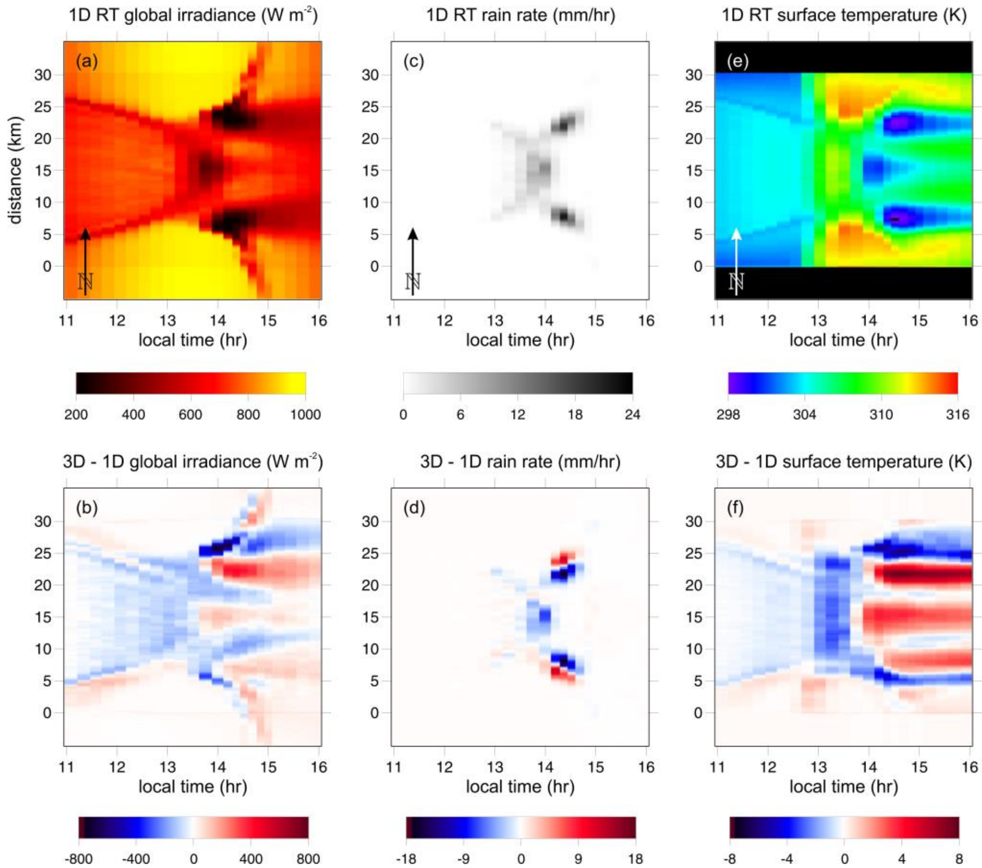

Figure 10. (a) Ensemble-average time series of global surface irradiance averaged longitudinally across the "averaging region", as indicted in ***Figure 8***, for simulations using regular 1D RT for "no synoptic wind" conditions. (b) Difference between (a) and corresponding values using parametrized 1D RT (referred to here as 3D RT). (c) and (d) are as in (a) and (b) except these are for surface rain rate. (e) and (f) are as in (a) and (b) except these are for surface temperature.

5. Results

Consider first the case of 'no synoptic wind". For 1D RT, clouds cast shadows directly beneath themselves and so lake breeze conditions should be very close to symmetric about the W-E centre of the isthmus. This is confirmed in ***Figure 10a*** which shows a Hovmöller-style plot of global surface irradiance averaged W-E across the domain as a function local time. The plot begins shortly after scattered shallow cumulus form inland of the lake breeze fronts; both of which are, at this time, ~4 km from the coasts. Conditions are symmetric throughout the simulation with irradiance minima occurring shortly after 14h00 along the breeze fronts, which have migrated to ~7 km inland. This coincides with maximum surface rain rate (***Figure 10c***) which, coupled with diminished surface solar heating, cools the surface (***Figure 10e***) almost shutting down the lake breezes. With areas of rain dying and moving coastward, with clouds extending out over water and lessening inland, mid-afternoon surface temperatures across most of the isthmus rise despite the Sun going down (***Figure 9***).

The lower row of panels in ***Figure 10*** show differences between the top row's 1D RT results and results for the simulations using parametrized 1D RT, which are referred to as "3D RT" in the plot titles only because they are meant to approximate 3D RT. The mild asymmetry between the north and south sides of the isthmus, as seen in ***Figure 10b***, is set-up by the shifting of cloud shadows in the direction of the south coast's breeze and counter to the north coast's breeze. A schematic of this is shown in ***Figure 11*** which shows why clouds, and ultimately rain, that form along the breeze fronts shift coastward for approximate 3D RT (cf. Gronemeier et al. 2017). This is confirmed by ***Figure 12*** and ***Figure 13*** which show that, near peak-breeze strength at 14h00, vertical wind speeds are generally weaker and cloud densities less for 3D RT. While these differences were the largest seen here, they would be of little concern to weather forecasters.

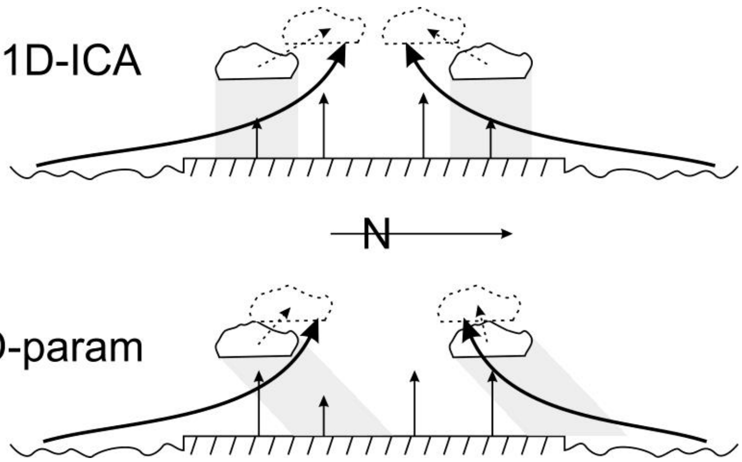

Figure 11. Schematic showing clouds forming along lake breeze fronts for both RT treatments for "no synoptic wind" conditions. For the 1D RT model, clouds that form along the breeze fronts cast shadows directly beneath themselves. They are drawn in the direction of the breezes due to surface heating just inland of them. For the south shore's breeze, this drawing inland is curtailed whilst heating remains to take place directly beneath clouds (when μ_0 is not too large). For the north breeze, heating beneath cloud also occurs but the breeze can be expected to be diminished due to cloud shadows cast further towards the coast.

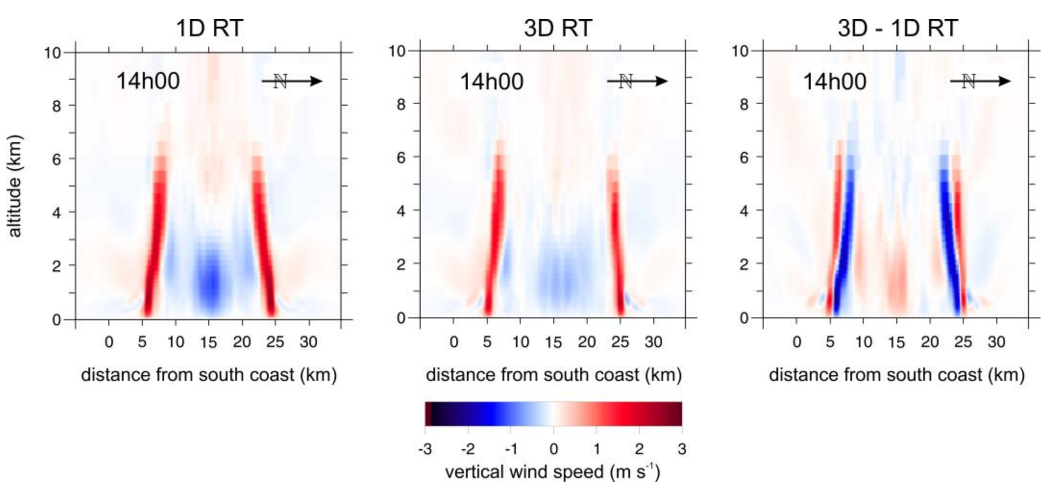

Figure 12. Longitudinal average cross-sections of vertical wind speed averaged across the "averaging region" shown in ***Figure 8*** for simulations using regular 1D RT, parametrized (3D) RT, and their differences at 14h00 local time. These are for "no synoptic wind" conditions.

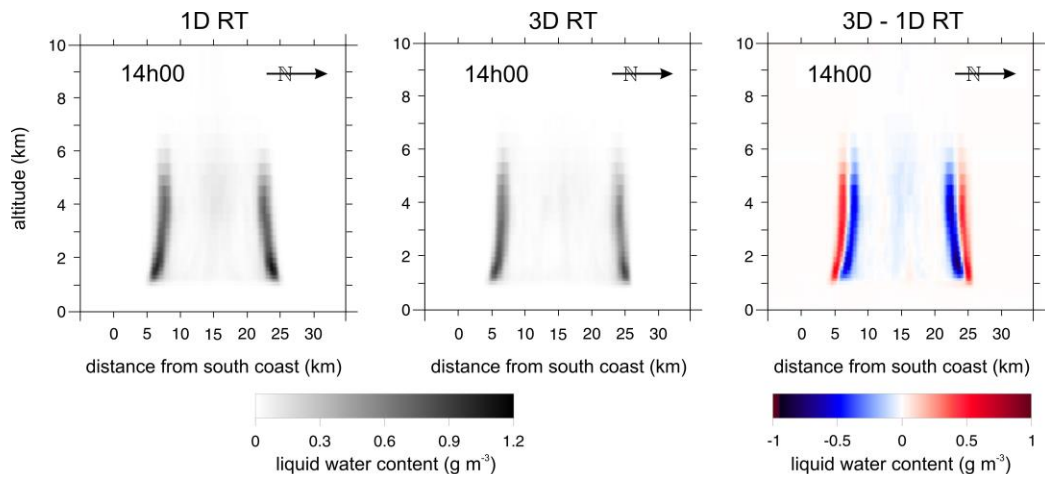

Figure 13. As in ***Figure 12*** except these show cloud liquid water contents.

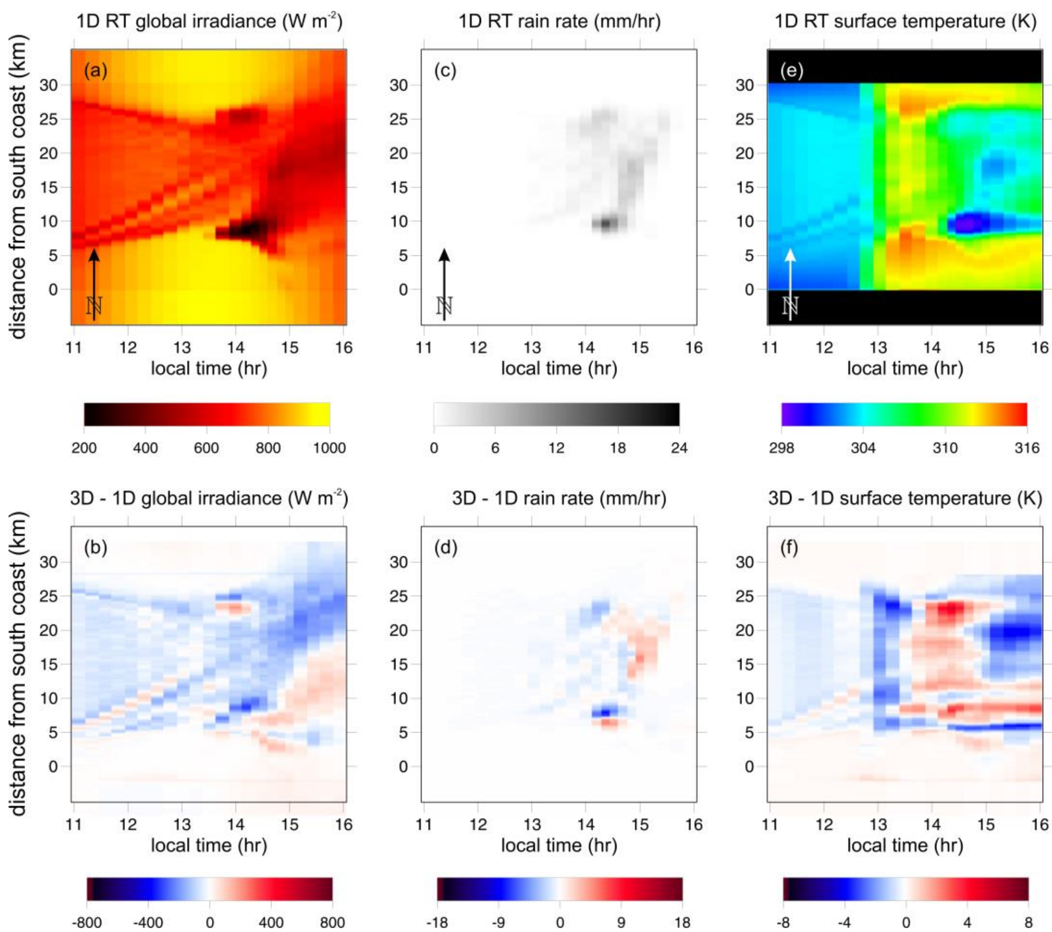

Figure 14. As in ***Figure 10*** but these are for SW synoptic winds.

Although lake breezes along the Great Lakes are common when synoptic winds are weak during high pressure conditions, they also occur during fair-weather conditions with south-westerly winds. ***Figure 14*** is a repeat of ***Figure 10*** for SW synoptic winds. It is immediately clear that for 1D-ICA RT the SW flow has upset the symmetry relative to no synoptic wind; especially the north shore breeze which is so diminished, fighting against the synoptic flow, that only a weak initial band of rain develops along its front. Differences in surface global irradiance, rain rate, and temperature affected by use of the 1D parametrization are also weakened relative to "no synoptic wind". What does develop, however, is enhanced rain, via enhanced convection (e.g., Veerman et al. 2020), near the centre of the isthmus at ~15h00 with notable subsequent surface cooling due to the combined effects of surface moistening and reduced irradiance, and north-easterly migration of rain thanks to synoptic wind. But as with no synoptic winds, differences between 1D-ICA and the pseudo-3D RT parametrization are minor and unlikely to alter short-term weather forecasts.

Table 1 lists domain-averages and standard deviations of surface global irradiance, temperature, and rain rate when 1D and 3D RT simulations are integrated across all "averaging domains" (see ***Figure 8***) between 11h00 and 16h00 local time, for all synoptic wind experiments. In all cases, 3D RT leads to 2% - 6% less surface irradiance due mostly to thicker, albeit slightly fewer, clouds. The impact of thicker but few clouds is also manifest in enhanced standard deviations of surface irradiance across the domain; direct-beam variations throttling global irradiances between very large and small values (see ***Figure 6***). While surface temperatures for 1D and 3D RT differ negligibly, fractional areas with rain decrease slightly when 3D RT is used, with rain intensity both increasing and decreasing, though by no more than $\pm 6\%$.

Table 1. Domain-averages, domain-standard deviations, and fractional areas averaged over all ensemble members from 11h00 to 16h00 local time.

	global irradiance ($W m^{-2}$)		**surface temperature (K)**		**surface rain rate > 0 ($mm hr^{-1}$)**	
	no synoptic wind					
	1D	**3D**	**1D**	**3D**	**1D**	**3D**
domain-average	714.1	698.8	306.2	306.2	2.98	2.84
domain-stdev	255.1	305.2	4.8	4.7	9.34	9.02
area	-	-	-	-	0.21	0.17
	W					
	1D	**3D**	**1D**	**3D**	**1D**	**3D**
domain-average	748.8	701.8	306.7	306.4	2.91	2.81
domain-stdev	227.1	289.1	4.7	4.7	8.86	8.71
area	-	-	-	-	0.17	0.17
	NW					
	1D	**3D**	**1D**	**3D**	**1D**	**3D**
domain-average	747.4	706.3	306.7	306.5	2.76	2.83
domain-stdev	227.4	285.9	4.8	4.7	8.50	8.79
area	-	-	-	-	0.18	0.17
	SW					
	1D	**3D**	**1D**	**3D**	**1D**	**3D**
domain-average	745.9	705.7	306.8	306.6	2.90	3.06
domain-stdev	232.7	291.6	4.8	4.8	8.72	9.30
area	-	-	-	-	0.18	0.17

6. Summary and discussion

An algorithm was presented that makes simple, and numerically efficient, adjustments to spatial distributions of diffuse- and direct-beam surface solar irradiances as predicted by the standard 1D-ICA RT framework, thus bringing them into better alignment with results from 3D radiative transfer (RT) models. The modified-ICA is best applied in well-resolved NWP or cloud-resolving models. The motivation for this was to help NWP modellers decide if it is necessary to replace the ubiquitous 1D solar RT model, with a 3D counterpart, before expending much effort on implementing computationally expensive 3D RT models in NWP models.

A smoothing filter is applied to the 2D distribution of surface diffuse irradiances simulated by a 1D-ICA model to approximate lateral diffusion of radiation below clouds. The breadth of the filter increases with cloud altitude, beginning with no smoothing for surface fog. Using high-resolution cloudy-sky data (cf. Barker and Davies 1989; Hogan et al. 2019) it was shown that this simple alteration typically increases the Pearson correlation coefficient between 1D-ICA and truly 3D RT modelled diffuse-beam irradiances by 0.1 to 0.2. Direct-beam irradiances for the modified-ICA are set by tracing a single ray from the centre of each surface cell toward the Sun, accumulating cloud optical depth along them, and applying Beer's law. This positions cloud shadows accurately and typically increases the Pearson correlation coefficient between 1D-ICA and truly 3D RT direct-beam irradiances by 0.65 at $\theta_0 = 75°$ and 0.5 at $\theta_0 = 60°$; correctly, no improvement occurs at $\theta_0 \approx 0°$ as 1D RT cloud shadows are already positioned properly.

While the modified-ICA and standard 1D-ICA have equal domain-average diffuse irradiances, which, strictly speaking, is incorrect (cf. Welch and Wielicki 1985), the modified-ICA's direct irradiances are normalized by forcing its domain-average *global* irradiance to equal the standard 1D-ICA's. This neglect of differences between 1D-ICA and 3D mean surface irradiances should be minor, for as several studies have shown (e.g., Pincus et al. 1999; Di Giuseppe and Tompkins 2003; O'Hirok and Gautier 2005; Ham et al. 2014; Barker et al. 2015, 2016; Hogan et al. 2019; Gristey et al. 2020), these differences are typically less than 10 W m^{-2} (or ~2%). Moreover, atmospheric heating rates for the modified-ICA are identical to those produced by the standard 1D-

ICA, which differ only slightly from their true 3D counterparts (see ***Figure 2*** and Hogan et al. 2019).

To gauge the importance of taking proper account of cloud shadows, the GEM NWP model used the standard- and modified-ICAs to simulate lake breezes. Lake breezes were focussed on because they are set-up when land surfaces, adjacent to cool lakes, are warmed by solar irradiance. They often lead to lines of cumulus clouds and localized convective precipitation; both of which feedback on the circulation that spawned them (e.g., Jakub and Mayer 2017). Since GEM, like all NWP models, employees 1D-ICA models whose clouds cast shadows at nadir, regardless of θ_0, the standard- and modified-ICAs enabled testing of whether NWP model simulations of lake breezes are sensitive to location of shadows cast by clouds on land surfaces.

In summary, while GEM's simulations of lake breeze-dependent cloud and surface meteorological conditions respond in clear and explainable ways when its standard 1D-ICA solar RT model is replaced by its modified version, which captures important features of 3D RT, the impacts are unlikely to alter local weather forecasts. Given the strong dependence of lake breezes on local solar heating, it is hard to imagine other short-term weather scenarios being significantly more sensitive to 3D solar RT effects (e.g., for deep convection, differences in radiative heating due to 1D and 3D RT models are likely to be greatly overshadowed by other processes). Hence, there is, as yet, no compelling reason for NWP models, which are used for short-range weather forecasting, to abandon their efficient 1D-ICA RT models. It is too early to tell, however, if this statement applies to seasonal weather and long-term climate predictions, where *cumulative effects* of 1D-ICA biases might be important (see Hogan and Bozzo 2018). In the meantime, NWP modellers might be advised to consider employment of methods that aim to improve numerical efficiency of 1D-ICA RT (e.g., Barker and Li 2019; Barker et al. 2020).

Acknowledgements

In the short-term, data used for this study can be obtained from the corresponding author. By the time of publication, ECCC will have an official data repository from which data used here will be downloadable.

References

Barker, H. W. and J. A. Davies, 1989: Multiple reflections across a linear discontinuity in surface albedo. *Int. J. Clim.*, **9**, 203-214.

Barker, H. W., G. L. Stephens, and Q. Fu, 1999: The sensitivity of domain-averaged solar fluxes to assumptions about cloud geometry. *Q. J. R. Meteorol. Soc.*, **125**, 2127-2152.

Barker, H. W. and A. Marshak, 2001: Inferring optical depth of broken clouds above green vegetation using surface solar radiometric measurements. *J. Atmos. Sci.*, **58**, 2989-3006.

Barker, H. W., R. K. Goldstein, and D. E. Stevens, 2003: Monte Carlo simulation of solar reflectances for cloudy atmospheres. *J. Atmos. Sci.*, **60**, 1881-1894.

Barker, H. W. and A. Davis, 2005: Approximation Methods in Atmospheric 3D Radiative Transfer, Part 2: Unresolved Variability and Climate. pg. 343-384 in *Three-dimensional Cloud Structure and Radiative Transfer*. Eds. A. Marshak and A., Davis. Springer-Verlag, 686pp.

Barker, H. W., S. Kato, and T. Wehr, 2012: Computation of Solar Radiative Fluxes by 1D and 3D Methods using Cloudy Atmospheres Inferred from A-train Satellite Data. *Surveys in Geophys.* **33**, 657-676.

Barker, H. W., J. N. S. Cole, J. Li, B. Yi, and P. Yang, 2015: Estimation of Errors for Two-Stream Approximations of the Solar Radiative Transfer Equation for Cloudy Atmospheres. *J. Atmos. Sci.*, **72**, 4053-4074.

Barker, H. W., J. N. S. Cole, J. Li, and K. von Salzen, 2016: A Parametrization of 3D Subgrid-scale Clouds for Conventional GCMs: Assessment using A-Train Satellite Data and Solar Radiative Transfer Characteristics. *J. Adv. Model. Earth Syst.* DOI: 10.1002/2015MS000601.

Barker, H. W., Z. Qu, S. Belair, S. Leroyer, J. A. Milbrandt, P. A. Vaillancourt, 2017: Scaling Properties of Observed and Simulated Satellite Visible Radiances. *J. Geophys. Res.*, 122, 9413– 9429, doi:10.1002/2017JD027146.

Barker, H. W. and J. Li, 2019: Accelerating radiative transfer calculations for high-resolution atmospheric models. *Q. J. R. Meteorol. Soc.*, **145**, 2046–2069.

Barker, H. W., Z. Qu, V. Dhanraj, and J. N. S. Cole, 2020: Partial validation of a lossy compression approach to computing radiative transfer in cloud system-resolving models. *Q. J. R. Meteorol. Soc.*, **146**, 1–20. https://doi.org/10.1002/qj. 3922

Cole, J. N. S., H. W. Barker, Z., Qu, N., Villefranque, and M. W. Shephard, 2023 : Broadband Radiative Quantities for the EarthCARE Mission: The ACM-COM and ACM-RT Products. *Atmospheric Measurement Techniques*, **16**, 4271–4288.

Côté, J., S. Gravel, A. Méthot, A. Patoine, M. Roch, and A. Staniforth, 1998: The operational CMC–MRD Global Environmental Multiscale (GEM) model. Part I: Design considerations and formulation. *Mon. Wea. Rev.*, **126**, 1373–1395.

Das, P. K., 1980: Numerical simulation of the Indian monsoon. *Proc. Indian Academy of Sci. - Earth and Planet. Sci.*, **89**, 159-177.

Dehghan, A., Z. Mariani, S. Leroyer, P. Joe, D. Sills. S. Bélair, 2018: Evaluation of Modeled Lake Breezes Using an Enhanced Observational Network in Southern Ontario: Case Studies. *J. of Meteorol. and Climatol*., **57**, 1511–1534.

Di Giuseppe, F. and A. M. Tompkins, 2003: Effect of Spatial Organization on Solar Radiative Transfer in Three-Dimensional Idealized Stratocumulus Cloud Fields. *J. Atmos. Sci*., **60**, 1774-1794.

Estoque, M. A., 1961: A theoretical investigation of the sea breeze. *Q. J. R. Meteorol. Soc*., **87**, 136-146.

Girard, C., M. Desgagné, R. McTaggart-Cowan, J. Côté, M. Charron, S. Gravel, V. Lee, A. Patoine, A. Qaddouri, M. Roch, L. Spacek, M. Tanguay, P. A. Vaillancourt, and A. Zadra, 2014: Staggered Vertical Discretization of the Canadian Environmental Multiscale (GEM) model using a coordinate of the log-hydrostatic-pressure type. *Mon. Weather Rev*., **142**, 1183-1196. doi.org/10.1175/MWR-D-13-00255.1

Gristey, J. J., G. Feingold, I. B. Glenn, K. S. Schmidt, and H. Chen, 2020: Surface Solar Irradiance in Continental Shallow Cumulus Fields: Observations and Large-Eddy Simulation. *J. Atmos. Sci*., **77**, 1065–1080.

Gronemeier, T., F. Kanani-Sühring, and S. Raasch, 2017: Do Shallow Cumulus Clouds have the Potential to Trigger Secondary Circulations Via Shading? *Boundary-Layer Meteo*., **162**, 143–169.

Ham, S.-H., S. Kato, H. W. Barker, F. G. Rose, and S. Sun-Mack, 2015: Improving the modeling of shortwave radiation through the use of a 3D scene construction algorithm. *Q. J. R. Meteorol. Soc*., **141**, 1870–1883. DOI: 10.1002/qj.2491.

Hogan, R. J. and A. Bozzo, 2018: A flexible and efficient radiationscheme for the ECMWF model. *J. Adv. Model. Earth Sys*.,**10**, 1990-2008. https://doi.org/10.1029/2018MS001364

Hogan, R. J., M. D. Fielding, H. W. Barker, N. Villefranque, and S. A. K. Schafer, 2019: Entrapment: An important mechanism to explain the shortwave 3D radiative effect of clouds. *J. Atmos. Sci*., 76, 2123-2141.

Iacono, M. J., J. S. Delamere, E. J. Mlawer, M. W. Shephard, S. A. Clough, and W. D. Collins, 2008: Radiative forcing by long-lived greenhouse gases: Calculations with the AER radiative transfer models, *J. Geophys. Res*., **113**, D13103, doi:10.1029/2008JD009944.

Illingworth, A., + others, 2015: THE EARTHCARE SATELLITE: The next step forward in global measurements of clouds, aerosols, precipitation and radiation. *Bull. Am. Met. Soc*., **96**, 1311-1332. DOI:10.1175/BAMS-D-12-00227.1.

Jakub, F. and B. Mayer, 2017: The role of 1-D and 3-D radiative heating in the organization of shallow cumulus convection and the formation of cloud streets. *Atmos. Chem. Phys*., **17**, 13317–13327. https://doi.org/10.5194/acp-17-13317-2017

Marshak, A, A. B. Davis, W. J. Wiscombe, and R. F. Cahalan, 1995: Radiative smoothing in fractal clouds. *J. Geophys. Res*., **100**, 26 247–26 261.

McTaggart-Cowan, R., Vaillancourt, P. A., Zadra, A., Chamberland, S., Charron, M., Corvec, S., Milbrandt, J. A., Paquin-Ricard, D., Patoine, A., Roch, M., Separovic, L., and Yang, J., 2019: Modernization of atmospheric physics parameterization in Canadian NWP. *J. Adv. Model. Earth Syst*., **11**, 3593–3635, https://doi.org/10.1029/2019MS001781.

Milbrandt, J. A., Bélair, S., Faucher, M., Vallée, M., Carrera, M. L., and Glazer, A., 2016: The pan-Canadian high resolution (2.5km) deterministic prediction system, *Weather Forecast.*, **31**, 1791–1816, https://doi.org/10.1175/WAF-D-16-0035.1.

O'Hirok, W. and C. Gautier, 2005: The impact of model resolution on differences between independent column approximation and Monte Carlo estimates of shortwave surface irradiance and atmospheric heating rate., *J. Atmos. Sci.*, **62**, 2939–2951, https://doi.org/10.1175/JAS3519.1.

Pincus, R., S. A. McFarlane, and S. A. Klein, 1999: Albedo bias and the horizontal variability of clouds in subtropical marine boundary layers: Observations from ships and satellites. *J. Geophys. Res*., **104**, 6183-6191.

Qu, Z., D. P. Donovan, H. W., Barker, J. N. S., Cole, and M. Shephard, 2023: Numerical model generation of test frames for pre-launch studies of EarthCARE's retrieval algorithms and data management system. *Atmospheric Measurement Techniques*, **16**, 2319-2331.

Schumann, U. A. Dörnbrack, and B. Mayer, 2002: Cloud-shadow effects on the structure of the convective boundary layer. *Meteorologische Zeitschrift*, **11**, 285-294.

Tijhuis, M., B. van Stratum, and C. C. van Heerwaarden, 2022: An efficient parameterization for surface 3d radiative effects in large-eddy simulations. *Earth and Space Science Open Archive*, 17. https://doi.org/10.1002/essoar.10511758.

Veerman, M. A., X. Pedruzo-Bagazgoitia,F. Jakub,J. Vilà-Guerau de Arellano,C. C. van Heerwaarden, 2020: Three-Dimensional Radiative Effects By Shallow Cumulus Clouds on Dynamic Heterogeneities Over a Vegetated Surface. *J. Advances Mod. Earth Sys*., **12**, e2019MS00199, https://doi.org/10.1029/2019MS001990

Wapler, K. and Mayer, B., 2008: A fast three-dimensional approximation for the calculation of surface irradiance in Large-Eddy Simulation Models, *J. Appl. Meteorol. Clim*., **47**, 3061–3071, https://doi.org/10.1175/2008JAMC1842.1.

Welch, R. M and B. A. Wielicki, 1985: A radiative parameterization of stratocumulus cloud fields. *J. Atmos. Sci.*, **42**, 2888-2897.